Quantum-number-projected generator-coordinate-method analysis of low-lying states in nuclei around mass 80

Koji Higashiyama[1,*] and Naotaka Yoshinaga[2,†]

[1]*Department of Physics, Chiba Institute of Technology, Narashino, Chiba 275-0023, Japan*
[2]*Department of Physics, Saitama University, Saitama City 338-8570, Japan*

The quantum-number-projected generator coordinate method (QNPGCM) is applied to the neutron-rich Ge and Se isotopes where the monopole and quadrupole pairing plus quadrupole-quadrupole interaction is employed as an effective interaction. The energy spectra calculated with both axial and triaxial deformations are compared to the shell-model results and the experimental data. In both cases, the QNPGCM reproduces well the energy levels of the even-spin yrast states. However, the QNPGCM results by only assuming axial deformations are not satisfactory enough to reproduce the energy levels of the quasi-γ bands. Taking account of triaxial deformations is essentially important to describe the yrast and quasi-γ bands simultaneously.

I. INTRODUCTION

The atomic nuclei exhibit, in general, prolate deformations, when some nucleons are added to a spherical closed-shell nucleus. On the other hand, they become oblate shapes when some nucleons are extracted from the spherical closed-shell nucleus. Neutron-rich $_{32}$Ge and $_{34}$Se isotopes in the mass $A \approx 80$ region have several valence protons outside the closed-shell $Z = 28$ and several neutron holes with respect to the close-shell $N = 50$. As a result, these nuclei are neither prolate nor oblate and may have triaxial deformations.

There are many theoretical and experimental studies to investigate the triaxial characteristics of the even-even nuclei in the mass $A \approx 80$ region [1–12]. These results show that the γ degree of freedom plays an important role in describing these nuclei. After the triaxial deformation has been established, a further question is whether this triaxiality has a γ-soft (γ-unstable) or γ-rigid deformation. There are two simple elementary models that describe these triaxialitys. The γ-soft model of Wilets and Jean [13] has nearly flat potential minima in the γ direction, whereas the rigid triaxial model of Davydov and Filippov [14] has deep potential minima for some γ deformation. The characteristics that distinguish between the γ-rigid and the γ-soft nuclei can be seen in the energy staggering of even-odd spin states in the quasi-γ band [15].

The experimental evidence for rigid triaxiality in ^{76}Ge was reported by Toh *et al.* [5]. In the paper, the staggering pattern of the energy levels in the quasi-γ band suggested γ-rigid deformation. A similar experimental result was also reported on the neighboring nucleus, ^{74}Ge [8]. The triaxiality of the low-lying states in Ge and Se isotopes was theoretically in-

vestigated in terms of the multiquasiparticle triaxial projected shell model (TPSM) [6]. In order to reproduce the experimental data for both the yrast and the quasi-γ bands of ^{76}Ge, it was shown that a fixed triaxial deformation with $\gamma = 30°$ is required in the TPSM calculation, which is consistent with the result of the rigid triaxial model [14]. The low-lying states in the even-even $^{72–82}$Ge isotopes were calculated in the framework of nuclear density functional theory [7]. The analysis indicated that the mean-field potential of ^{76}Ge was γ soft and did not support the interpretation of γ-rigid deformation.

One of the purposes in the present paper is to investigate the important role played by the triaxial degree of freedom for the low-lying states especially for the quasi-γ bands. In order to achieve this end, we apply the quantum-number-projected generator coordinate method (QNPGCM) to ^{78}Ge, ^{76}Ge, ^{80}Se, and ^{78}Se. The model space and the effective Hamiltonian were defined in our previous shell-model studies in this region [16,17]. In the present QNPGCM scheme, wave functions in each neutron or proton space are constructed separately, and many-body wave functions for an even-even nucleus are constructed as linear combinations of them. Intrinsic states among identical nucleons are determined from the Nilsson BCS model [18,19]. In order to clarify the triaxiality of the low-lying states in Ge and Se isotopes, we calculate the potential-energy surface (PES) with the quadrupole deformations (β, γ). Energy spectra and $E2$ transition rates are also calculated by assuming axial and triaxial deformations and compared to the shell-model results and the experimental data. The QNPGCM results reveal important effects of the triaxial components.

The paper is organized as follows. In Sec. II, the framework of the QNPGCM and its form of the effective interactions in the model space are presented. In Sec. III the QNPGCM calculations are carried out for the even-even nuclei ^{78}Ge, ^{76}Ge, ^{80}Se, and ^{78}Se. The principal results are summarized in Sec IV.

_____

*koji.higashiyama@it-chiba.ac.jp
†yoshinaga@phy.saitama-u.ac.jp

II. THEORETICAL FRAMEWORK

The previous QNPGCM studies [20–23] made it clear that, for a description of the nuclear collective and single-particle motions in a transitional region, the angular momentum of the neutron system (I_ν) and that of the proton system (I_π) should be projected out separately, and the total spin I is constructed by the angular momentum coupling. Thus, in the present QNPGCM scheme, the angular momentum projection is performed separately in each neutron or proton space. To generate functions for the QNPGCM, we employ the Nilsson BCS intrinsic states $|\Phi_\tau(\beta_\tau, \gamma_\tau)\rangle$ for either the neutron ($\tau = \nu$) or the proton ($\tau = \pi$) system, where β_τ and γ_τ indicate axial and triaxial quadrupole deformations, respectively. Neither angular momentum I_τ nor the valence nucleon number N_τ are good quantum numbers for the conventional Nilsson BCS intrinsic state [18,19]. However, in the present scheme, we construct the intrinsic state that conserves the valence nucleon number N_τ.

The ρth QNPGCM wave function with angular momentum I_τ and its projection M_τ in either neutron ($\tau = \nu$) or proton space ($\tau = \pi$) is given by

$$\left|\Psi^{(\tau)}_{I_\tau M_\tau \rho}\right\rangle = \sum_i \sum_{K=-I_\tau}^{I_\tau} \mathcal{F}^{I_\tau i}_{K\rho} \hat{P}^{I_\tau}_{M_\tau K} |\Phi_\tau(\beta_i, \gamma_i)\rangle, \quad (1)$$

where $\hat{P}^{I_\tau}_{M_\tau K}$ is the spin projection operator [24] and i stands for a representative point with deformation (β, γ). The weight functions $\mathcal{F}^{I_\tau i}_{K\rho}$ and the QNPGCM energies $E_{I_\tau \rho}$ are determined by solving the Hill-Wheeler equation for each deformation (β_i, γ_i),

$$\sum_j \sum_{K'=-I_\tau}^{I_\tau} [\langle \Phi_\tau(\beta_i, \gamma_i)|\hat{H}_\tau \hat{P}^{I_\tau}_{KK'}|\Phi_\tau(\beta_j, \gamma_j)\rangle$$
$$\times E_{I_\tau \rho}\langle \Phi_\tau(\beta_i, \gamma_i)|\hat{P}^{I_\tau}_{KK'}|\Phi_\tau(\beta_j, \gamma_j)\rangle]\mathcal{F}^{I_\tau j}_{K'\rho} = 0, \quad (2)$$

under the normalization condition,

$$\left\langle \Psi^{(\tau)}_{I_\tau M_\tau \rho}\middle|\Psi^{(\tau)}_{I'_\tau M'_\tau \rho'}\right\rangle = \delta_{I_\tau I'_\tau}\delta_{\rho\rho'}\delta_{M_\tau M'_\tau}, \quad (3)$$

where $\hat{H}_\tau$ represents the interaction among like nucleons. Finally, a many-body wave function for an even-even nucleus can be made from the angular momentum coupling of neutron and proton wave functions as

$$|\Psi_{IM}(I_\nu \rho I_\pi \sigma)\rangle = \left[\left|\Psi^{(\nu)}_{I_\nu \rho}\right\rangle \otimes \left|\Psi^{(\pi)}_{I_\pi \sigma}\right\rangle\right]^{(I)}_M$$
$$\equiv \sum_{M_\nu M_\pi} (I_\nu M_\nu I_\pi M_\pi|IM)\left|\Psi^{(\nu)}_{I_\nu M_\nu \rho}\right\rangle\left|\Psi^{(\pi)}_{I_\pi M_\pi \sigma}\right\rangle, \quad (4)$$

where I and M are the total spin and its projection, respectively, and $(I_\nu M_\nu I_\pi M_\pi|IM)$ stands for a Clebsch-Gordan coefficient. Here the symbol $\otimes$ denotes the angular momentum coupling of the neutron angular momentum I_ν and the proton angular momentum I_π to the total angular momentum I.

The Nilsson BCS intrinsic state $|\Phi_\tau(\beta, \gamma)\rangle$ appearing in Eq. (1) is constructed by the following procedure. First we consider the Nilsson Hamiltonian for either neutron space

($\tau = \nu$) or proton space ($\tau = \pi$),

$$\hat{h}^{(\tau)}_{\text{Nilsson}} = \sum_{jm} \varepsilon_j c^\dagger_{jm\tau} c_{jm\tau}$$
$$- \frac{\hbar\omega\beta}{b^2}\left[\cos\gamma \hat{Q}_{0\tau} - \frac{\sin\gamma}{\sqrt{2}}(\hat{Q}_{2\tau} + \hat{Q}_{-2\tau})\right], \quad (5)$$

where ε_j represents the single-particle energy in the orbital j, $c^\dagger_{jm\tau}$ ($c_{jm\tau}$) represents a nucleon creation (annihilation) operator, and (j, m) represents a set of quantum numbers necessary to specify the spherical single-particle state (n, ℓ, j, m). The notation of the Nilsson Hamiltonian follows those of Refs. [20,21]. The quadrupole operator $\hat{Q}_{M\tau}$ is defined by

$$\hat{Q}_{M\tau} = \sum_{j_1 j_2} Q_{j_1 j_2}[c^\dagger_{j_1\tau}\tilde{c}_{j_2\tau}]^{(2)}_M$$
$$= \sum_{j_1 j_2 m_1 m_2} Q_{j_1 j_2}(j_1 m_1 j_2 m_2|2M)c^\dagger_{j_1 m_1 \tau}\tilde{c}_{j_2 m_2 \tau}, \quad (6)$$

with

$$\tilde{c}_{jm\tau} = (-1)^{j-m}c_{j-m\tau}, \quad (7)$$

$$Q_{j_1 j_2} = -\frac{\langle j_1|r^2 Y^{(2)}|j_2\rangle}{\sqrt{5}}. \quad (8)$$

In the present scheme, harmonic-oscillator basis states with the oscillator parameter $b = \sqrt{\hbar/M\omega}$ are used as the single-particle basis states. The major shell separation energy $\hbar\omega$ (in units of MeV) is assumed to follow the conventional relation,

$$\hbar\omega = 41A^{-1/3}. \quad (9)$$

The Nilsson Hamiltonian in Eq. (5) is diagonalized in terms of the spherical single-particle basis state $|jm\tau\rangle = c^\dagger_{jm\tau}|-\rangle$ as

$$\hat{h}^{(\tau)}_{\text{Nilsson}}|\alpha\tau\rangle = e_{\alpha\tau}|\alpha\tau\rangle, \quad (10)$$

where $|\alpha\tau\rangle$ and $e_{\alpha\tau}$ are the Nilsson single-particle state and Nilsson single-particle energy, respectively, and α is an additional quantum number required to completely specify the state. Here eigenenergies are sorted in increasing order as $e_{\alpha_1\tau} \leqslant e_{\alpha_2\tau} \leqslant \cdots$. The Nilsson single-particle state $|\alpha\tau\rangle = b^\dagger_{\alpha\tau}|-\rangle$ is related with the spherical basis state $|jm\tau\rangle$ as

$$|\alpha\tau\rangle = \sum_{jm} F_{jm,\alpha\tau}|jm\tau\rangle. \quad (11)$$

Using the Nilsson single-particle creation operator $b^\dagger_{\alpha\tau}$, the many-body Nilsson states are written as

$$|\Phi_\tau(\beta, \gamma)\rangle = \prod_{\alpha=1}^{N_\tau} b^\dagger_{\alpha\tau}|-\rangle, \quad (12)$$

where N_τ represents the valence particle number. The positive parity is always ensured as a good quantum number for the many-body Nilsson states.

Next, in order to include the pairing correlation, we perform the Bardeen-Cooper-Schrieffer (BCS) calculation for the Nilsson single-particle states. The BCS Hamiltonian consists of the Nilsson single-particle energies and the monopole

pairing (MP) interaction,

$$\hat{h}_{\text{BCS}}^{(\tau)} = \sum_{\alpha>0} e_{\alpha\tau}(b_{\alpha\tau}^{\dagger}b_{\alpha\tau} + b_{\bar{\alpha}\tau}^{\dagger}b_{\bar{\alpha}\tau})$$
$$-G_{0\tau}\sum_{\alpha,\beta>0} b_{\alpha\tau}^{\dagger}b_{\bar{\alpha}\tau}^{\dagger}b_{\bar{\beta}\tau}b_{\beta\tau}, \qquad (13)$$

where $b_{\alpha\tau}$ represents a Nilsson single-particle annihilation operator and $\bar{\alpha}$ indicates the time reversal of state α. The strength of the MP interaction is taken to be the same as used in the shell-model calculation. By solving the BCS equations, we obtain the Nilsson BCS intrinsic state,

$$\left|\Psi_{\text{BCS}}^{(\tau)}(\beta,\gamma)\right\rangle = \prod_{\alpha>0}(u_{\alpha\tau} + v_{\alpha\tau}b_{\alpha\tau}^{\dagger}b_{\bar{\alpha}\tau}^{\dagger})|-\rangle, \qquad (14)$$

where $u_{\alpha\tau}$ and $v_{\alpha\tau}$ are the unoccupied and occupied amplitudes for state α, respectively. As the Nilsson BCS intrinsic state $|\Psi_{\tau}^{(\text{BCS})}(\beta,\gamma)\rangle$ does not conserve the valence particle number N_{τ}, a state with a good particle number is obtained by using the following relation:

$$|\Phi_{\tau}(\beta,\gamma)\rangle = \mathcal{N}\left(\sum_{\alpha>0}\frac{v_{\alpha\tau}}{u_{\alpha\tau}}b_{\alpha\tau}^{\dagger}b_{\bar{\alpha}\tau}^{\dagger}\right)^{N_{\tau}/2}|-\rangle, \qquad (15)$$

where $\mathcal{N}$ denotes the normalization. Then, the QNPGCM wave function in Eq. (1) is generated using this number conserved BCS state. For some deformation points, the BCS equation does not have any solutions. In such a situation (normal phase), the Nilsson intrinsic state in Eq. (12) is used.

As an effective two-body interaction, we employ the pairing plus quadrupole-type interaction. The effective shell-model Hamiltonian is written as

$$\hat{H} = \hat{H}_{\nu} + \hat{H}_{\pi} + \hat{H}_{\nu\pi}, \qquad (16)$$

where $\hat{H}_{\nu}$, $\hat{H}_{\pi}$, and $\hat{H}_{\nu\pi}$ represent the neutron interaction, the proton interaction, and the neutron-proton interaction, respectively. The interaction among like nucleons $\hat{H}_{\tau}$ ($\tau = \nu$ or π) consists of spherical single-particle energies, MP interaction, quadrupole-pairing (QP) interaction, and quadrupole-quadrupole (QQ) interaction,

$$\hat{H}_{\tau} = \sum_{jm}\varepsilon_{j\tau}c_{jm\tau}^{\dagger}c_{jm\tau}$$
$$-G_{0\tau}\hat{P}_{\tau}^{\dagger(0)}\hat{P}_{\tau}^{(0)} - G_{2\tau}\hat{P}_{\tau}^{\dagger(2)}\cdot\tilde{P}_{\tau}^{(2)} - \kappa_{\tau}:\hat{Q}_{\tau}\cdot\hat{Q}_{\tau}:, \quad (17)$$

where : : denotes normal ordering and the operator $\hat{Q}_{\tau}$ is the quadrupole operator defined by Eq. (6). The MP operator $P_{\tau}^{\dagger(0)}$ and the QP operators $P_{M\tau}^{\dagger(2)}$, $\tilde{P}_{M\tau}^{(2)}$ are defined as

$$\hat{P}_{\tau}^{\dagger(0)} = \sum_{j}\frac{\sqrt{2j+1}}{2}\hat{A}_{0\tau}^{\dagger(0)}(jj), \qquad (18)$$

$$\hat{P}_{M\tau}^{\dagger(2)} = \sum_{j_1j_2}Q_{j_1j_2}\hat{A}_{M\tau}^{\dagger(2)}(j_1j_2), \qquad (19)$$

$$\tilde{P}_{M\tau}^{(2)} = (-)^{M}[\hat{P}_{-M\tau}^{\dagger(2)}]^{\dagger}, \qquad (20)$$

where the value of $Q_{j_1j_2}$ is given by Eq. (8). The creation operator of a pair of nucleons in the orbitals j_1 and j_2 with

TABLE I. Adopted single-particle energies $\varepsilon_{j\tau}$ for neutron holes ($\tau = \nu$) or proton particles ($\tau = \pi$) in units of MeV.

j	$0g_{9/2}$	$1p_{1/2}$	$1p_{3/2}$	$0f_{5/2}$
$\varepsilon_{j\nu}$	0.0	0.5	1.0	3.0
$\varepsilon_{j\pi}$	3.3	1.1	0.6	0.0

a total angular momentum J and its projection M is defined as

$$\hat{A}_{M\tau}^{\dagger(J)}(j_1j_2) = \sum_{m_1m_2}(j_1m_1j_2m_2|JM)c_{j_1m_1\tau}^{\dagger}c_{j_2m_2\tau}^{\dagger}$$
$$= [c_{j_1\tau}^{\dagger}c_{j_2\tau}^{\dagger}]_{M}^{(J)}. \qquad (21)$$

The interaction between neutrons and protons $\hat{H}_{\nu\pi}$ is taken as

$$\hat{H}_{\nu\pi} = -\kappa_{\nu\pi}\hat{Q}_{\nu}\cdot\hat{Q}_{\pi}, \qquad (22)$$

where the operator $\hat{Q}_{\tau}$ is the quadrupole operator. The detailed framework of the model is reported in Refs. [16,25].

Finally, the effective Hamiltonian in Eq. (16) is diagonalized in terms of the many-body wave functions in Eq. (4) as

$$\hat{H}\left|I_{\eta}^{\pi}\right\rangle = E\left(I_{\eta}^{\pi}\right)\left|I_{\eta}^{\pi}\right\rangle, \qquad (23)$$

where $|I_{\eta}^{\pi}\rangle$ is the normalized eigenvector for the ηth state with total spin I and parity π and $E(I_{\eta}^{\pi})$ is the eigenenergy for state $|I_{\eta}^{\pi}\rangle$. Here angular momentum projection M is abbreviated.

III. NUMERICAL RESULTS

For the nuclei in the mass $A \approx 80$ region, several valence neutron holes and valence proton particles are coupled to the doubly closed ^{78}Ni core. Since the valence neutron holes (proton particles) occupy the $0f_{5/2}$, $1p_{3/2}$, $1p_{1/2}$, and $0g_{9/2}$ orbitals, we take into account the full $28 \leqslant N(Z) \leqslant 50$ configuration space for neutrons (protons) where valence neutrons (protons) are treated as holes (particles).

For the single-particle energies and the interaction strengths, we have used exactly the values given by the set of equations used in the previous shell-model study of $A \approx 80$ nuclei [16] without any further modification. The single-particle energies $\varepsilon_{j\tau}$ ($\tau = \nu$ or π) employed in the present calculations are listed in Table I.

In order to reproduce overall spectra of the even-even and odd-mass nuclei in the mass $A \approx 80$ region, linear dependences of the interaction strengths on the valence neutron and/or proton numbers was introduced. The determined set of interactions is as follows (G_0 of MP interaction in units of MeV, and G_2 of the QP interaction, and κ of the QQ interaction, both in units of MeV/b^4),

$$G_{0\nu} = 0.16 + 0.03\bar{N}_{\nu},$$
$$G_{2\nu} = 0.042 + 0.008\bar{N}_{\nu},$$
$$\kappa_{\nu} = 0.31 - 0.01\bar{N}_{\nu} - 0.015N_{\pi},$$
$$G_{0\pi} = 0.30 - 0.01\bar{N}_{\nu} - 0.01N_{\pi},$$
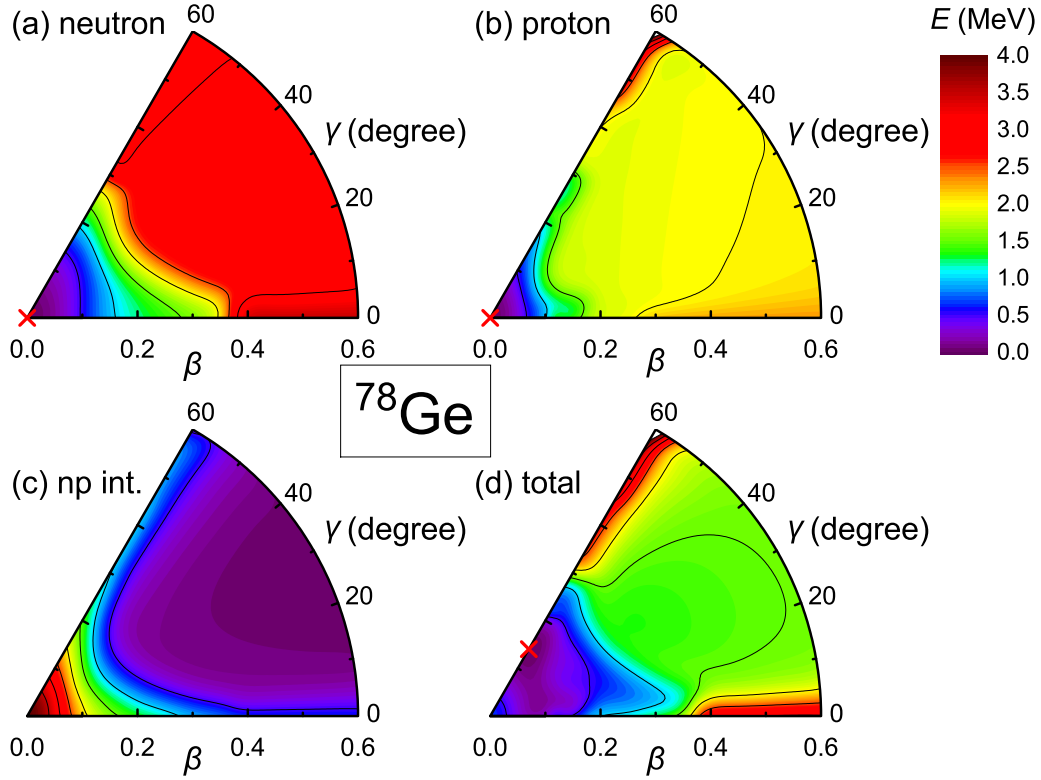$$G_{2\pi} = 0.06 - 0.002\bar{N}_{\nu} - 0.006N_{\pi},$$

FIG. 1. The contour plot of the energy gain on the β-γ plane calculated for ^{78}Ge with (a) the neutron interaction, (b) the proton interaction, (c) the QQ interaction between neutrons and protons, and (d) the total Hamiltonian. The contour line separation energy is 0.5 MeV. The point where the energy gain takes its minimum is indicated by the symbol $\times$ (cross).

$$\kappa_\pi = 0.08 + 0.015\bar{N}_\nu - 0.005N_\pi,$$
$$\kappa_{\nu\pi} = -0.20. \qquad (24)$$

Here $\bar{N}_\nu$ represents the number of valence neutron holes, and N_π represents the number of valence proton particles.

In the present paper we carry out the numerical analysis in terms of the QNPGCM. Their results are compared with those in the shell model. As for the single-particle energies and the strengths of the effective interaction, we use the same values given above. The detailed framework of the shell model is presented in Ref. [16].

A. Potential-energy surface

Using the set of the interaction strengths determined above, we calculate the PES on the β-γ plane for the Nilsson BCS states. The potential energy for either the neutron system ($\tau = \nu$) or the proton system ($\tau = \pi$) is defined as

$$E_\tau(\beta, \gamma) = \langle \Phi_\tau(\beta, \gamma)|\hat{H}_\tau|\Phi_\tau(\beta, \gamma)\rangle, \qquad (25)$$

where $\hat{H}_\tau$ represents the interaction among like nucleons in Eq. (17) and $|\Phi_\tau(\beta, \gamma)\rangle$ is the Nilsson BCS state in Eq. (15).

In this paper, the QNPGCM wave functions are constructed in each neutron or proton space separately, and the many-body wave function for an even-even nucleus is constructed as linear combinations of the wave functions in Eq. (4). Thus, the present QNPGCM includes the many-body wave functions made by different deformations of the neutron and proton spaces. In order to examine underlying physics, we now cal-

culate the PES for the neutron-proton interaction assuming that they have same deformations, i.e., $(\beta, \gamma) = (\beta_\nu, \gamma_\nu) = (\beta_\pi, \gamma_\pi)$. The potential energy between neutrons and protons is defined as

$$E_{\nu\pi}(\beta, \gamma) = -\kappa_{\nu\pi} \sum_M (-1)^M Q_{M\nu}(\beta, \gamma)Q_{-M\pi}(\beta, \gamma), \qquad (26)$$

with

$$Q_{M\tau}(\beta, \gamma) = \langle \Phi_\tau(\beta, \gamma)|\hat{Q}_{M\tau}|\Phi_\tau(\beta, \gamma)\rangle. \qquad (27)$$

Using Eqs. (25) and (26), the potential energy for the total Hamiltonian is defined as

$$E(\beta, \gamma) = E_\nu(\beta, \gamma) + E_\pi(\beta, \gamma) + E_{\nu\pi}(\beta, \gamma). \qquad (28)$$

Figure 1(a) and 1(b), respectively, show the contour plots of the PESs for neutron and proton interactions of ^{78}Ge. In each neutron or proton space, the minimum of the PES exhibits zero deformation ($\beta = 0$) and almost no barrier in the γ direction. Concerning the β direction, the PES for the proton space shows a shallower slope compared with that for the neutron space.

In Fig. 1(c), the contour plots of the PES for the neutron-proton interaction are presented. In contrast to the neutron and proton spaces, the potential energy becomes maximum at zero deformation and decreases monotonically as β deformation increases. This difference arises from the treatment of the valence neutrons and protons. In the present paper valence neutrons are treated as holes, and valence protons are
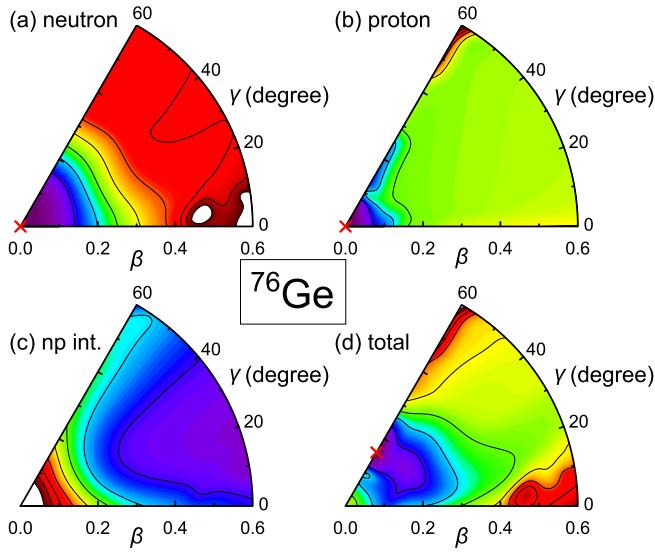
FIG. 2. The same as Fig. 1 but for ^{76}Ge.

treated as particles. Thus, the quadrupole interaction strength between neutrons and protons $\kappa_{\nu\pi}$ is taken as negative.
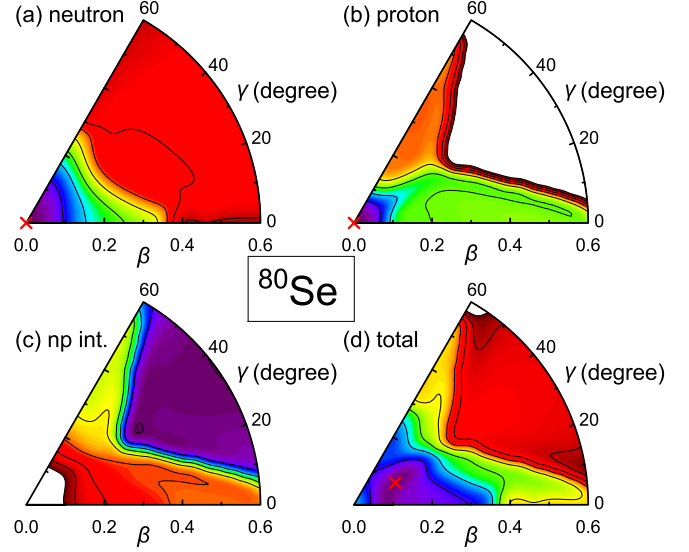
In Fig. 1(d), the contour plots of the PES in Eq. (28) are presented. A minimum of the PES appears at deformation $(\beta, \gamma) = (0.14, 60°)$, and the minima are very flat in the direction of the γ degree of freedom. This means that ^{78}Ge exhibits γ-soft triaxiality in the low-lying structure.

Figure 2 shows the contour plots of the PES for ^{76}Ge. Like ^{78}Ge, the energy minima are located at spherical shapes for both neutron and proton spaces. The present calculation also shows that the potential energy between neutrons and protons is maximum at zero deformation and gradually decreases as deformation β increases. Although the total potential-energy minimum for the total Hamiltonian appears at deformation $(\beta, \gamma) = (0.16, 60°)$, the energy surfaces are soft with respect to the γ direction. The previous studies suggested that ^{76}Ge may be a rare example of a nucleus exhibiting γ-rigid deformation in their low-lying structure [5,6]. However, the present result of the PES does not support the interpretation of γ-rigid triaxiality.

Figures 3 and 4 show the contour plots of the PES for ^{80}Se and ^{78}Se, respectively. The physical situation for these nuclei deviates from the cases of Ge isotopes. For both nuclei, the proton PESs present areas drawn in white color on the upper right side. In these areas, the Nilsson BCS model fails in giving numerical solutions, and the Nilsson intrinsic state is used to calculate the potential energy. The effect of the unsolved BCS equations is also visible in the PESs for the neutron-proton interaction, which are rather flat around these regions. Concerning ^{78}Se, the potential energy for the total Hamiltonian is very shallow in the γ direction, although the energy has its minimum for prolate deformation. As for ^{80}Se, triaxial minimum is seen, but the PES shows the γ softness similar to ^{78}Se.

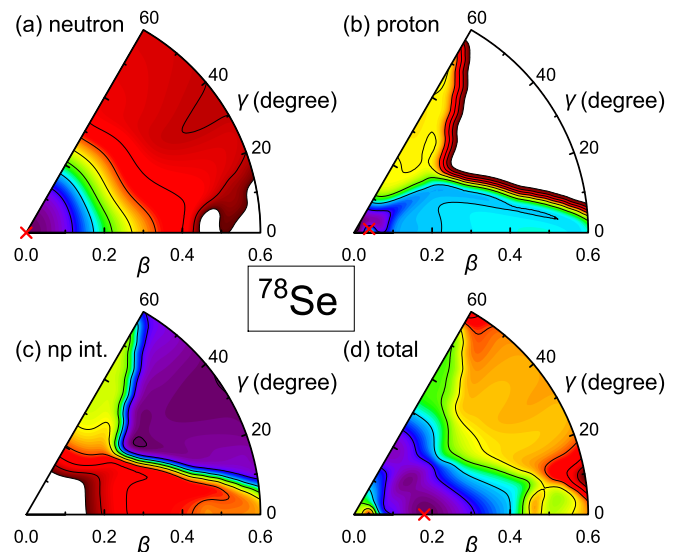### B. Energy spectra

In order to see the effect of triaxially deformed shapes explicitly, the QNPGCM calculations are carried out in two

cases: (i) triaxial deformations (nine deformation points) with $\beta = 0.10, 0.20, 0.30$, $\gamma = 10°, 30°, 50°$; (ii) only axial deformations (49 points) with $\beta = 0.00, 0.02, 0.04, \ldots, 0.48$, and $\gamma = 0°, 60°$.

In Fig. 5, the theoretical energy spectra in the triaxial QNPGCM and the axial QNPGCM are compared with the experimental data for ^{78}Ge. The energy spectrum of the shell model taken from Ref. [16] is also shown in this figure. In both cases of triaxial and axial deformations, not only the low-lying yrast sequence is almost perfectly described, but also a sudden decrease in the level spacing between 6_1^+ and 8_1^+ states in the yrast band is well reproduced. As for other excited states, the QNPGCM calculation performed by assuming triaxial deformations is in good agreement with the shell-model results especially for the 2_2^+, 3_1^+, 5_1^+, and 7_1^+ states, which are members of the quasi-γ band. However, their energy levels

FIG. 3. The same as Fig. 1 but for ^{80}Se.

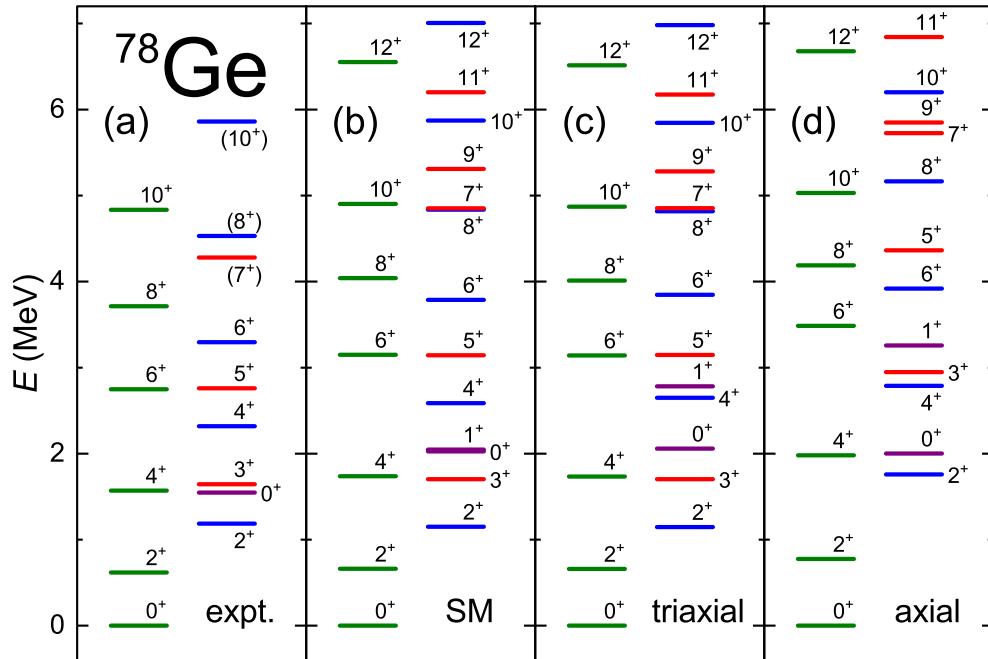FIG. 4. The same as Fig. 1 but for ^{78}Se.

FIG. 5. Comparison of the experimental energy spectrum with those in various models for ^{78}Ge. (a) Experimental energy levels, taken from Refs. [3,11,26]. (b) Calculated energy levels in the shell model [16], (c) in the triaxial QNPGCM, and (d) in the axial QNPGCM.

calculated by assuming only axial deformations appear higher in energy than the shell-model ones.

In Fig. 6, the theoretical energy spectra in the triaxial and axial QNPGCM are compared with the shell-model results and the experimental data for ^{76}Ge. The triaxial QNPGCM calculations well reproduce the correct positions of the even-spin yrast states as well as the 2_2^+, 3_1^+, 4_2^+, 5_1^+, 6_2^+, 7_1^+, and 8_2^+ states in the quasi-γ band. Concerning the axial QNPGCM calculation, a good correspondence with the shell-model results is achieved for the energy levels of the yrast states. However, the axial QNPGCM result is not satisfactory enough to describe the energy levels of the quasi-γ band.
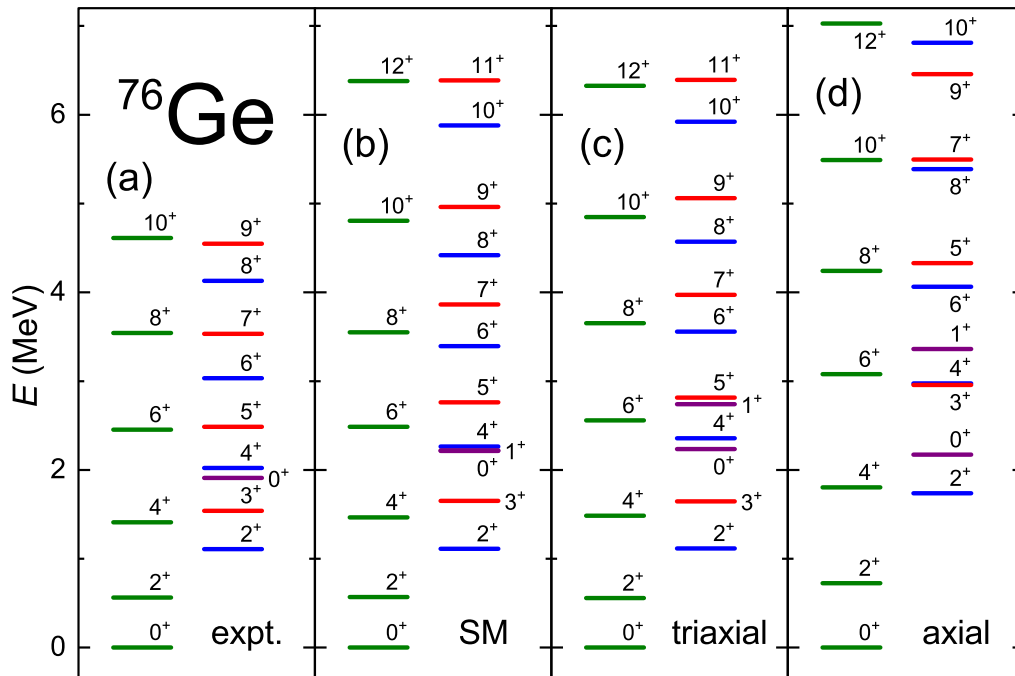

FIG. 6. The same as Fig. 6 but for ^{76}Ge. The experimental data are taken from Refs. [5,27].
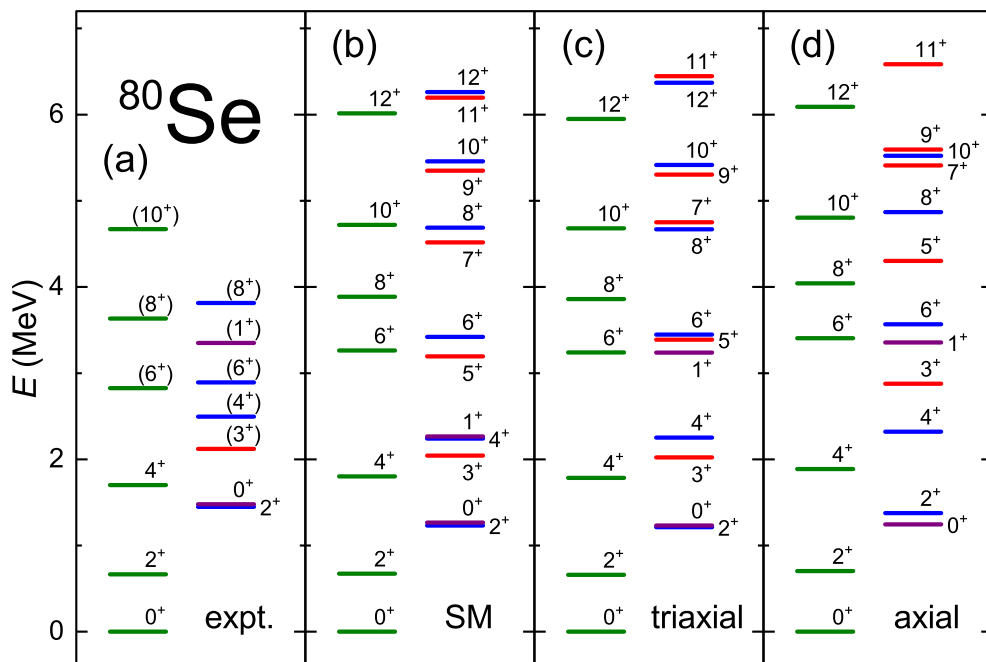
FIG. 7. The same as Fig. 6 but for ^{80}Se. The experimental data are taken from Ref. [28].

Figures 7 and 8 show the theoretical spectra for ^{80}Se and ^{78}Se, respectively, compared with the experimental data. Like Ge isotopes, the triaxial QNPGCM calculations almost perfectly reproduce the energy levels in the shell model. With respect to the even-spin states of both the yrast band and the quasi-γ band, the axial QNPGCM gives better agreement with the shell-model results than those of Ge isotopes. However, concerning the odd-spin states, there is a large discrepancy

between the energy levels in the axial QNPGCM and shell-model results.

Apparently, for all the nuclei the QNPGCM calculations performed by assuming triaxial deformations are in excellent agreement with the shell-model results. However, the description of the odd-spin states in the quasi-γ band is poorly reproduced when assuming only the axially symmetric shape. This means that the triaxial components play an essential role in the description of these states in the quasi-γ band.
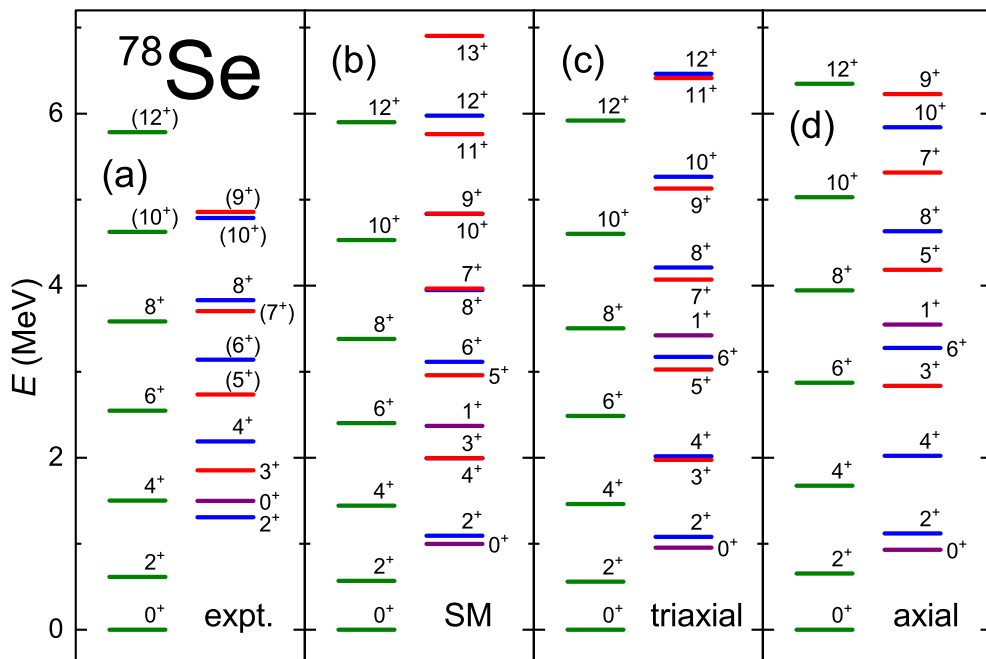

FIG. 8. The same as Fig. 6 but for ^{78}Se. The experimental data are taken from Ref. [26].
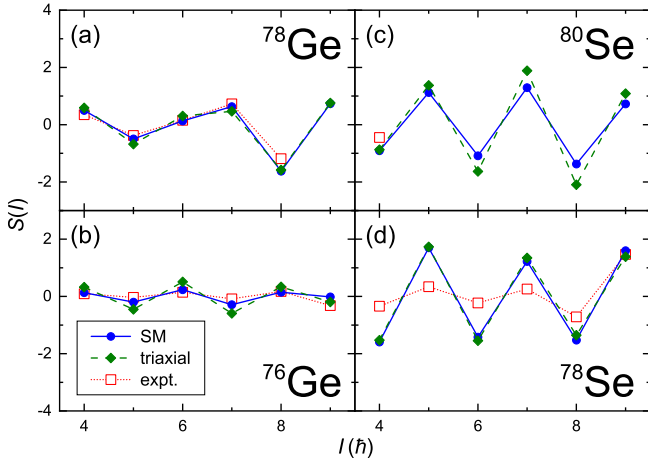
FIG. 9. Comparison of the theoretical staggering parameters $S(I)$ for the quasi-γ bands in (a) ^{78}Ge, (b) ^{76}Ge, (c) ^{80}Se, and (d) ^{78}Se with experimental data. The filled circles, and the filled diamonds represent the parameters in the shell model and in the triaxial QNPGCM, respectively. The open squares represent the experimental data, calculated by using the excitation energies in Refs. [3,5,11,26,26–28].

In order to examine the staggering pattern of the energy levels in the quasi-γ band, we calculate the staggering parameter [15]. The staggering parameter $S(I)$ is defined as

$$S(I) = \frac{[E(I) - E(I-1)] - [E(I-1) - E(I-2)]}{E(2_1^+)}, \quad (29)$$

where $E(I)$ is the eigenenergy for the state in the quasi-γ band with total spin I.

In Fig. 9, theoretical staggering parameters $S(I)$ for the quasi-γ bands in the triaxial QNPGCM are compared with the shell-model results and the experimental ones. For ^{78}Ge, ^{76}Ge, and ^{78}Se, the even-odd staggering of the $S(I)$ values is observed in experiment. Concerning Ge isotopes, the shell-model calculations almost perfectly reproduce the experimental ones, especially the phase irregularity occurring around total spin $I = 7$ in ^{78}Ge. For ^{78}Se, the staggering amplitude in the shell model is larger compared with the experimental ones, but the staggering pattern is in phase. The triaxial QNPGCM calculations successfully reproduce the shell-model results.

Since 5_1^+ and 7_1^1 states for ^{80}Se are not measured in experiment, the staggering parameter is obtained only for the total spin $I = 4$, which becomes negative. The theoretical $S(4)$ values in both the shell model and the triaxial QNPGCM are smaller than the experimental ones, but there exists a one-to-one correspondence between the theoretical and experimental levels.

The energy staggering of even-odd spin states in the quasi-γ band of ^{78}Ge was considered as evidence for γ-rigid triaxiality. As shown in Fig. 9 the staggering pattern is out of phase with that in Se isotopes. However, in the present paper good agreements between theoretical staggering patterns and experimental ones are clearly seen, although the total potential energy for ^{78}Ge is very shallow in the γ direction. This fact
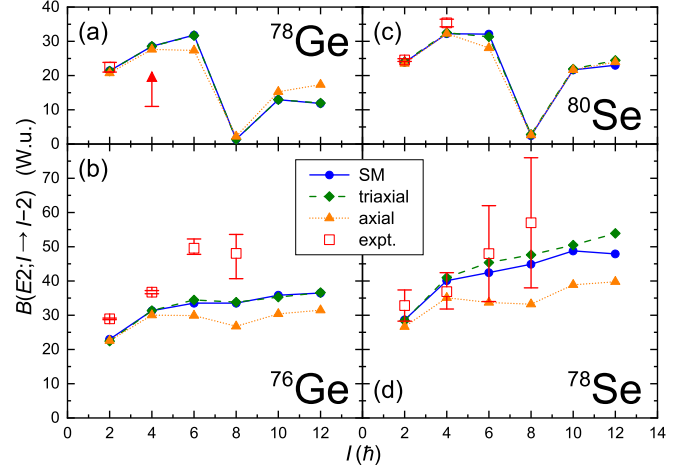

FIG. 10. Comparison of the theoretical $B(E2)$ values for the yrast states of (a) ^{78}Ge, (b) ^{76}Ge, (c) ^{80}Se, and (d) ^{78}Se with experimental data. The filled circles, the filled diamonds, and the filled triangles represent the transitions in the shell model, in the triaxial QNPGCM, and in the axial QNPGCM, respectively. The open squares represent the experimental data, taken from Refs. [2,10,29–32].

implies that calculating the staggering parameter is insufficient to distinguish between the γ-rigid and the γ-soft nuclei.

C. $E2$ transitions and electric quadrupole moments

The $E2$ transition rate is calculated as

$$B(E2; I_\eta^\pi \to J_\xi^\pi) = \frac{1}{2I+1} \left| \langle J_\xi^\pi \| \hat{T}(E2) \| I_\eta^\pi \rangle \right|^2, \quad (30)$$

where $|I_\eta^\pi\rangle$ is the normalized eigenvector in Eq. (23). Here the $E2$ transition operator is defined as

$$\hat{T}(E2; M) = e_\nu \hat{Q}_{M\nu} + e_\pi \hat{Q}_{M\pi}, \quad (31)$$

where e_τ ($\tau = \nu$ or π) represents the effective charge of the nucleon and $\hat{Q}_{M\tau}$ is the quadrupole operator defined by Eq. (6) with the oscillator parameter $b = 1.005A^{1/6}$ fm. The effective charges are assumed to follow the conventional relation $e_\pi = (1 + \delta)e$ and $e_\nu = -\delta e$, and the adopted values are $e_\nu = -0.65e$ and $e_\pi = 1.65e$, which are taken from Ref. [16].

In Fig. 10, the $B(E2)$ values for the yrast states in the shell model [16] are compared with those in the axial QNPGCM and the triaxial QNPGCM. The experimental $B(E2)$ values are also shown in this figure. In ^{78}Ge and ^{80}Se, the shell-model results exhibit sudden decreases in the $B(E2)$ values between the 6_1^+ and the 8_1^+ states. This anomalous behavior is attributed to a band crossing between the ground-state band and the aligned neutron $(0g_{9/2})^2$ band [16]. Concerning the QNPGCM results, it is found that theoretical $E2$ transition rates in both the triaxial and the axial QNPGCM agree well with the shell-model results. In ^{76}Ge and ^{78}Se, the shell-model results gradually increase as total spin I goes up. The triaxial QNPGCM calculations successfully reproduce these shell-model behaviors. However, the axial QNPGCM fails in reproducing the $B(E2)$ values in the shell model. These discrepancies may suggest that the deformation obtained by the

TABLE II. Comparison of the absolute $B(E2)$ values (in Weisskopf units) obtained by the shell model (SM) and the triaxial QNPGCM (QNPGCM) with the experimental data (Expt.). The experimental data are taken from Refs. [27,31,33]. No experimental data are available for ^{78}Ge.

$I_i^\pi \rightarrow I_f^\pi$	^{78}Ge SM	QNPGCM	^{76}Ge SM	QNPGCM	Expt.	^{80}Se SM	QNPGCM	Expt.	^{78}Se SM	QNPGCM	Expt.
$2_1^+ \rightarrow 2_1^+$	32.7	31.8	33.8	32.3	$29.9_{-0.8}^{+0.3}$	28.4	27.4	$14.0_{-1.4}^{+1.7}$	29.3	35.5	20 ± 4
$2_2^+ \rightarrow 0_1^+$	1.48	<0.01	1.54	2.02	$0.83_{-0.18}^{+0.20}$	<0.01	0.02	1.1 ± 0.1	<0.01	0.96	$0.65_{-0.15}^{+0.17}$
$3_1^+ \rightarrow 2_2^+$	39.5	39.2	40.1	40.6	20_{-3}^{+2}	20.9	21.3		18.3	17.0	
$3_1^+ \rightarrow 4_1^+$	22.4	22.4	20.4	21.1	14_{-3}^{+6}	11.0	10.4		14.3	13.1	
$3_1^+ \rightarrow 2_1^+$	2.54	0.53	2.63	3.50	0.50 ± 0.06	0.13	0.07		2.02	2.48	
$4_2^+ \rightarrow 2_2^+$	1.46	9.60	10.6	11.4	12.9 ± 0.3	17.3	19.4	$24.4_{-11.3}^{+6.2}$	28.2	29.0	
$4_2^+ \rightarrow 3_1^+$	0.19	1.77	0.57	0.02	24_{-5}^{+2}	0.04	0.10		0.22	0.86	
$4_2^+ \rightarrow 4_1^+$	0.89	4.60	9.87	11.0	22 ± 1	10.4	13.6		18.1	18.3	
$4_2^+ \rightarrow 2_1^+$	<0.01	0.30	<0.01	0.01	$2.8_{-0.7}^{+1.4}$	<0.01	0.01	$0.005_{-0.005}^{+1.06}$	0.09	0.13	
$0_2^+ \rightarrow 2_2^+$	0.01	0.02	0.63	<0.01		62.6	63.0	$1.2_{-1.2}^{+0.5}$	89.7	92.2	
$0_2^+ \rightarrow 2_1^+$	0.20	0.22	<0.01	0.13		0.47	0.63	$7.0_{-1.1}^{+1.2}$	4.87	5.44	

axial QNPGCM scheme is not satisfactory enough to describe the even-spin yrast states. The triaxial components play an essential role in the description of the low-lying states.

In Table II, the $B(E2)$ values in low-lying states calculated by the shell model and the triaxial QNPGCM are compared with the experimental data. Unfortunately, very few experimental data are available for ^{80}Se and ^{78}Se, and no data are available for ^{78}Ge. The basic features of the experimental data are well reproduced except for the transitions of $4_2^+ \rightarrow 3_1^+$ in ^{76}Ge and $0_2^+ \rightarrow 2_1^+$ in ^{80}Se, which are smaller than those in the shell model. It is noted that a good agreement between the triaxial QNPGCM results and those in the shell model is achieved for all the nuclei.

The electric quadrupole moment is calculated as

$$Q(I_\eta^\pi) = \langle I_\eta^\pi I_\eta^\pi | \hat{Q}_0 | I_\eta^\pi I_\eta^\pi \rangle, \qquad (32)$$

where the electric quadrupole operator is given by

$$\hat{Q}_M = \sqrt{\frac{16\pi}{5}} (e_\nu \hat{Q}_{M\nu} + e_\pi \hat{Q}_{M\pi}). \qquad (33)$$

The quadrupole operator $\hat{Q}_M$, the effective charges, and the oscillator parameter are taken to be the same as used for the

$E2$ transition rates. The electric quadrupole moments obtained by the shell model and the triaxial QNPGCM for the 2_1^+, 2_2^+, and 4_1^+ states are shown in Table III together with the experimental data. There are some disagreements between the theoretical quadrupole moments and the experimental data. In particular, for ^{76}Ge and ^{78}Se the theoretical quadrupole moments are positive for the 2_1^+ states, whereas the opposite behavior is shown in the experimental values. Even though these theoretical quadrupole moments are different in their signs from those of ^{78}Ge and ^{80}Se, the basic features of the potential energy for the total Hamiltonian are the same for all the nuclei.

In order to interpret the QNPGCM results, we calculate relative $B(E2)$ values between the low-lying states. In Table IV, the relative $B(E2)$ values in low-lying states calculated by the shell model and the triaxial QNPGCM are compared with those in the O(6) limit of the interacting boson model (IBM) [35]. For all the nuclei, the shell model gives the results almost identical to the O(6) limit, which is known to describe γ-soft nuclei [35–37]. Concerning the triaxial QNPGCM results, the relative $B(E2)$ values are well reproduced except for the ratio from the 0_2^+ state of ^{78}Ge. The nucleus ^{78}Ge has fewer valence neutrons and protons compared with the other

TABLE III. Comparison of the electric quadrupole moments (in eb) obtained by the shell model (SM) and the triaxial QNPGCM (QNPGCM) with the experimental data (Expt.). No experimental data are available for ^{78}Ge.

States	^{78}Ge SM	QNPGCM	^{76}Ge SM	QNPGCM	Expt.	^{80}Se SM	QNPGCM	Expt.	^{78}Se SM	QNPGCM	Expt.
2_1^+	−0.038	−0.035	+0.122	+0.152	-0.19 ± 0.06[a] -0.24 ± 0.02[b]	−0.187	−0.209	-0.31 ± 0.07[c] $-0.20_{-0.02}^{+0.03}$[d]	+0.186	+0.206	-0.22 ± 0.07[c] -0.20 ± 0.07[e]
2_2^+	+0.041	+0.037	−0.123	−0.153	$+0.26_{-0.05}^{+0.02}$[b]	+0.184	+0.205	$+0.40 \pm 0.02$[d]	−0.161	−0.178	$+0.17 \pm 0.09$[e]
4_1^+	−0.067	−0.068	+0.017	+0.027	$-0.26_{-0.07}^{+0.01}$[b]	−0.210	−0.223	$-0.64_{-0.05}^{+0.08}$[d]	+0.229	+0.256	-0.68 ± 0.15[e]

[a]Taken from Ref. [1].
[b]Taken from Ref. [27].
[c]Taken from Ref. [34].
[d]Taken from Ref. [33].
[e]Taken from Ref. [31].

TABLE IV. Comparison of calculated relative $B(E2)$ values obtained by the SM and the triaxial QNPGCM with the predictions of the O(6) limit of the IBM [O(6)].

$I_i^\pi \to I_f^\pi$	^{78}Ge		^{76}Ge		^{80}Se		^{78}Se		O(6)
	SM	QNPGCM	SM	QNPGCM	SM	QNPGCM	SM	QNPGCM	
$2_2^+ \to 2_1^+$	100	100	100	100	100	100	100	100	100
$\to 0_1^+$	4.5	0.9	4.5	6.3	0.0	0.0	< 0.1	2.7	0
$3_1^+ \to 2_2^+$	100	100	100	100	100	100	100	100	100
$\to 4_1^+$	57	57	50	52	53	49	78	77	40
$\to 2_1^+$	6.4	1.3	6.4	8.6	0.6	0.3	11	15	0
$4_2^+ \to 2_2^+$	100	100	100	100	100	100	100	100	100
$\to 3_1^+$	13	18	5.4	0.1	0.2	0.5	0.8	3.0	0
$\to 4_1^+$	61	48	93	97	60	70	64	63	91
$\to 2_1^+$	0.1	3.1	< 0.1	0.1	0.0	0.1	0.3	0.5	0
$0_2^+ \to 2_2^+$	6.6	6.8	100	< 0.1	100	100	100	100	100
$\to 2_1^+$	100	100	0.9	100	0.8	1.0	5.4	5.9	0

nuclei, ^{76}Ge, ^{80}Se, and ^{78}Se. The quadrupole collectivity is not so pronounced, and the single-particle nature still dominates. For an accurate description for such states, we need to expand the model space to include further single-particle degrees of freedom. This will be one of our next important projects.

IV. SUMMARY

In this paper the QNPGCM is applied to ^{78}Ge, ^{76}Ge, ^{80}Se, and ^{78}Se. In the present scheme, the proton and neutron wave functions are constructed separately by using the QNPGCM, and they are coupled through diagonalization of the total Hamiltonian. The effective Hamiltonian employed in this paper consists of the single-particle energies and the pairing plus quadrupole-quadrupole interaction, whose strengths were determined so as to describe the energy levels of the even-even and odd-mass nuclei in the previous shell-model study [16].

To clarify the triaxiality in the low-lying structure, it is desirable to calculate the total potential energy. For all the nuclei, the energy surfaces are soft with respect to the γ direction, which results in a different interpretation from the rigid triaxiality.

The theoretical energy spectra obtained by assuming axial and triaxial deformations are compared to the shell-model results and the experimental data. In both cases, the QNPGCM reproduces well the energy levels of the even-spin states in the yrast bands. However, the QNPGCM results for axial deformations are not satisfactory enough to reproduce the energy levels of the quasi-γ bands.

The $E2$ transition rates along the yrast bands are also calculated, and an excellent agreement between the $B(E2)$ values in the triaxial QNPGCM and shell-model results is clearly seen. Concerning the axial deformation, there are a few discrepancies between the QNPGCM results and the shell-model ones. Taking account of triaxial deformations is essentially important to simultaneously describe the yrast and quasi-γ bands.

This physical situation is supported by further analyses, i.e., by calculation of the relative $B(E2)$ values for the low-lying states. Calculated relative $B(E2)$ values reproduce very well the results in the O(6) limit of the IBM, which is known to describe γ-soft nuclei. These results are in accord with the analysis of the total potential energy.

In the present paper the triaxiality of the low-lying states is investigated theoretically. The PES with the quadrupole deformations (β, γ) is found to be soft with regard to the γ deformation for all the nuclei considered here. It was reported in previous studies [38,39] that the model-independent sum rules construct the parameters Q and δ from the $E2$ transition rates of the low-lying states, which are related to the axial and triaxial quadrupole deformation parameters β and γ. In our future work we plan to calculate the Q and δ parameters with the use of the theoretical $E2$ transition rates and compare them with those obtained by the total potential energy.

[1] R. Lecomte, M. Irshad, S. Landsberger, P. Paradis, and S. Monaro, Evidence of a spherical to prolate shape transition in the germanium nuclei, Phys. Rev. C **22**, 1530 (1980).

[2] R. Lecomte, M. Irshad, S. Landsberger, G. Kajrys, P. Paradis, and S. Monaro, Coulomb-excitation studies of ^{70}Ge, ^{72}Ge, ^{74}Ge, and ^{76}Ge, Phys. Rev. C **22**, 2420 (1980).

[3] W.-T. Chou, D. S. Brenner, R. F. Casten, and R. L. Gill, Level lifetime measurements and the structure of neutron-rich ^{78}Ge, Phys. Rev. C **47**, 157 (1993).

[4] Y. Toh, T. Czosnyka, M. Oshima, T. Hayakawa, H. Kusakari, M. Sugawara, Y. Hatsukawa, J. Katakura, N. Shinohara, and M. Matsuda, Coulomb excitation of ^{74}Ge beam, Eur. Phys. J. A **9**, 353 (2000).

[5] Y. Toh, C. J. Chiara, E. A. McCutchan, W. B. Walters, R. V. F. Janssens, M. P. Carpenter, S. Zhu, R. Broda, B. Fornal, B. P. Kay, F. G. Kondev, W. Królas, T. Lauritsen, C. J. Lister, T. Pawłat, D. Seweryniak, I. Stefanescu, N. J. Stone, J. Wrzesiński, K. Higashiyama *et al.*, Evidence for rigid triaxial deformation at low energy in ^{76}Ge, Phys. Rev. C **87**, 041304(R) (2013).

[6] G. H. Bhat, W. A. Dar, J. A. Sheikh, and Y. Sun, Nature of γ deformation in Ge and Se nuclei and the triaxial projected shell model description, Phys. Rev. C **89**, 014328 (2014).

[7] T. Nikšić, P. Marević, and D. Vretenar, Microscopic analysis of shape evolution and triaxiality in germanium isotopes, Phys. Rev. C **89**, 044325 (2014).

[8] J. Sun, Z. Shi, X. Li, H. Hua, C. Xu, Q. Chen, S. Zhang, C. Song, J. Meng, X. Wu, S. Hu, H. Zhang, W. Liang, F. Xu, Z. Li, G. Li, C. He, Y. Zheng, Y. Ye, D. Jiang *et al.*, Spectroscopy of ^{74}Ge: From soft to rigid triaxiality, Phys. Lett. B **734**, 308 (2014).

[9] A. Ayangeakaa, R. Janssens, C. Wu, J. Allmond, J. Wood, S. Zhu, M. Albers, S. Almaraz-Calderon, B. Bucher, M. Carpenter, C. Chiara, D. Cline, H. Crawford, H. David, J. Harker, A. Hayes, C. Hoffman, B. Kay, K. Kolos, A. Korichi *et al.*, Shape coexistence and the role of axial asymmetry in ^{72}Ge, Phys. Lett. B **754**, 254 (2016).

[10] S. Mukhopadhyay, B. P. Crider, B. A. Brown, S. F. Ashley, A. Chakraborty, A. Kumar, M. T. McEllistrem, E. E. Peters, F. M. Prados-Estévez, and S. W. Yates, Nuclear structure of ^{76}Ge from inelastic neutron scattering measurements and shell model calculations, Phys. Rev. C **95**, 014327 (2017).

[11] A. M. Forney, W. B. Walters, C. J. Chiara, R. V. F. Janssens, A. D. Ayangeakaa, J. Sethi, J. Harker, M. Alcorta, M. P. Carpenter, G. Gürdal, C. R. Hoffman, B. P. Kay, F. G. Kondev, T. Lauritsen, C. J. Lister, E. A. McCutchan, A. M. Rogers, D. Seweryniak, I. Stefanescu, and S. Zhu, Novel $\Delta J = 1$ Sequence in ^{78}Ge: Possible Evidence for Triaxiality, Phys. Rev. Lett. **120**, 212501 (2018).

[12] J. Henderson, C. Y. Wu, J. Ash, B. A. Brown, P. C. Bender, R. Elder, B. Elman, A. Gade, M. Grinder, H. Iwasaki, B. Longfellow, T. Mijatović, D. Rhodes, M. Spieker, and D. Weisshaar, Triaxiality in selenium-76, Phys. Rev. C **99**, 054313 (2019).

[13] L. Wilets and M. Jean, Surface oscillations in even-even nuclei, Phys. Rev. **102**, 788 (1956).

[14] A. Davydov and G. Filippov, Rotational states in even atomic nuclei, Nucl. Phys. **8**, 237 (1958).

[15] N. Zamfir and R. Casten, Signatures of γ softness or triaxiality in low energy nuclear spectra, Phys. Lett. B **260**, 265 (1991).

[16] N. Yoshinaga, K. Higashiyama, and P. H. Regan, High-spin structure of neutron-rich Se, As, Ge, and Ga isotopes, Phys. Rev. C **78**, 044320 (2008).

[17] N. Yoshinaga and K. Higashiyama, Band structure of neutron rich Se and Ge isotopes, J. Phys.: Conf. Ser. **445**, 012032 (2013).

[18] M. Baranger and K. Kumar, Nuclear deformations in the pairing-plus-quadrupole model: (II). Discussion of validity of the model, Nucl. Phys. A **110**, 490 (1968).

[19] K. Kumar and M. Michel Baranger, Nuclear deformations in the pairing-plus-quadrupole model: (III). Static nuclear shapes in the rare-earth region, Nucl. Phys. A **110**, 529 (1968).

[20] K. Enami, K. Tanabe, and N. Yoshinaga, Generator coordinate method combined with exact triaxial spin projection: Application to the single-j shell model, Phys. Rev. C **63**, 044322 (2001).

[21] K. Enami, K. Tanabe, and N. Yoshinaga, Capability of the GCM calculation with spin and particle number projections for single j-shell model, Prog. Part. Nucl. Phys. **46**, 177 (2001).

[22] K. Enami, K. Tanabe, and N. Yoshinaga, Quantum-number-projected generator coordinate method and the shell model, Phys. Rev. C **65**, 064308 (2002).

[23] K. Enami, K. Higashiyama, K. Tanabe, and N. Yoshinaga, Quantum-number-projected generator coordinate method analysis of low-lying states in ^{130,132}Xe, Phys. Rev. C **66**, 047301 (2002).

[24] P. Ring and P. Schuck, *The Nuclear Many Body Problem* (Springer-Verlag, Berlin, 1980).

[25] K. Higashiyama, N. Yoshinaga, and K. Tanabe, Shell model study of backbending phenomena in Xe isotopes, Phys. Rev. C **65**, 054317 (2002).

[26] A. R. Farhan and B. Singh, Nuclear Data Sheets for $A = 78$, Nucl. Data Sheets **110**, 1917 (2009).

[27] A. D. Ayangeakaa, R. V. F. Janssens, S. Zhu, D. Little, J. Henderson, C. Y. Wu, D. J. Hartley, M. Albers, K. Auranen, B. Bucher, M. P. Carpenter, P. Chowdhury, D. Cline, H. L. Crawford, P. Fallon, A. M. Forney, A. Gade, A. B. Hayes, F. G. Kondev, Krishichayan *et al.*, Evidence for Rigid Triaxial Deformation in ^{76}Ge from a Model-Independent Analysis, Phys. Rev. Lett. **123**, 102501 (2019).

[28] B. Singh, Nuclear data sheets for $A = 80$, Nucl. Data Sheets **105**, 223 (2005).

[29] R. Schwengner, G. Winter, J. Döring, L. Funke, P. Kemnitz, E. Will, A. E. Sobov, A. D. Efimov, M. F. Kudojarov, I. K. Lemberg, A. S. Mishin, A. A. Pasternak, L. A. Rassadin, and I. N. Chugunov, Collective and two-particle excitations in ^{78}Se, Z. Phys. A **326**, 287 (1987).

[30] K.-H. Speidel, N. Benczer-Koller, G. Kumbartzki, C. Barton, A. Gelberg, J. Holden, G. Jakob, N. Matt, R. H. Mayer, M. Satteson, R. Tanczyn, and L. Weissman, Shell closure effects in the stable $^{74-82}$Se isotopes from magnetic moment measurements using projectile excitation and the transient field technique, Phys. Rev. C **57**, 2181 (1998).

[31] T. Hayakawa, Y. Toh, M. Oshima, A. Osa, M. Koizumi, Y. Hatsukawa, Y. Utsuno, J. Katakura, M. Matsuda, T. Morikawa, M. Sugawara, H. Kusakari, and T. Czosnyka, Projectile Coulomb excitation of ^{78}Se, Phys. Rev. C **67**, 064310 (2003).

[32] E. Padilla-Rodal, A. Galindo-Uribarri, C. Baktash, J. C. Batchelder, J. R. Beene, R. Bijker, B. A. Brown, O. Castaños, B. Fuentes, J. G. del Campo, P. A. Hausladen, Y. Larochelle, A. F. Lisetskiy, P. E. Mueller, D. C. Radford, D. W. Stracener, J. P. Urrego, R. L. Varner, and C.-H. Yu, $B(E2) \uparrow$ Measurements for Radioactive Neutron-Rich Ge Isotopes: Reaching the $N = 50$ Closed Shell, Phys. Rev. Lett. **94**, 122501 (2005).

[33] A. Kavka, C. Fahlander, A. Bäcklin, D. Cline, T. Czosnyka, R. Diamond, D. Disdier, W. Kernan, L. Kraus, I. Linck, N. Schulz, J. Srebrny, F. Stephens, L. Svensson, B. Varnestig, E. Vogt, and C. Wu, Coulomb excitation of ^{76,80,82}Se, Nucl. Phys. A **593**, 177 (1995).

[34] R. Lecomte, P. Paradis, J. Barrette, M. Barrette, G. Lamoureux, and S. Monaro, Measurement of the static quadrupole moments of the first 2^+ states in ^{76}Se, ^{78}Se, ^{80}Se, and ^{82}Se, Nucl. Phys. A **284**, 123 (1977).

[35] F. Iachello and A. Arima, *The Interacting Boson Model* (Cambridge University Press, Cambridge, UK, 1987).

[36] G. Puddu, O. Scholten, and T. Otsuka, Collective quadrupole states of Xe, Ba, and Ce in the interacting boson model, Nucl. Phys. A **348**, 109 (1980).

[37] R. Casten and P. Von Brentano, An extensive region of O(6)-like nuclei near $A = 130$, Phys. Lett. **152B**, 22 (1985).

[38] K. Kumar, Intrinsic Quadrupole Moments and Shapes of Nuclear Ground States and Excited States, Phys. Rev. Lett. **28**, 249 (1972).

[39] D. Cline, Nuclear shapes studied by coulomb excitation, Annu. Rev. Nucl. Part. Sci. **36**, 683 (1986).